



State Key Laboratory of Numerical Modeling for Atmospheric Sciences and Geophysical Fluid Dynamics (LASG), Institute of Atmospheric Physics (IAP), Chinese Academy of Sciences (CAS), P.O. Box 9804, Beijing 100029, China  
Tel: 86-10-82995323 Fax: 86-10-82995172 <http://www.lasg.ac.cn>

---

## The short oral presentation of my poster

Hello, ladies and gentlemen. I'm Shan Yin, a Ph.D. student from Institute of Atmospheric Physics, Chinese Academy of Science. It's a great honor for me to attend this school to learn from these outstanding scientists and colleagues and show my work. My poster is about the relationship between the preceding boreal winter Northern Hemisphere Annular Mode (NAM) and the spring extreme low temperature events in the north of eastern China. The results show that there exists a significantly inverse relationship between them. When the preceding winter NAM is stronger, there are less low temperature events in the north of eastern China and vice versa. The possible physical mechanism associated is the Eurasian snow cover. The details can be seen on my poster and I gratefully welcome comments and suggestions! Thank you!

Shan Yin

2011-9-13



State Key Laboratory of Numerical Modeling for Atmospheric Sciences and Geophysical Fluid Dynamics (LASG), Institute of Atmospheric Physics (IAP), Chinese Academy of Sciences (CAS), P.O. Box 9804, Beijing 100029, China  
Tel: 86-10-82995299 Fax: 86-10-82995172 <http://www.lasg.ac.cn>

---

Good afternoon, Ladies and gentleman,

My name is Fei Zheng, a PhD student from Institute of Atmospheric Physics, Chinese Academy of Sciences. It is really my great pleasure to attend CPS 8<sup>th</sup> international school to learn from all these outstanding scientists and colleagues.

My poster shows the negative correlation between the preceding boreal winter Southern Hemisphere Annular Mode (abbreviate as SAM) and spring rainfall in South China, and gives a possible mechanism for this relationship. SAM is the most important pattern of climate variability in the middle and high latitudes of the Southern Hemisphere. As its hemispheric-scale, SAM can impact climate world-widely. Discussing the relationship between SAM and climate in East Asian is helpful for climate forecasting.

Welcome to my poster for more details, and I am really hoping for your suggestions and comments.

Thank you.

# Theoretical Modelling of Stars

## - Determination of Physical Parameters of $\mu$ Cas

K. Bach<sup>1</sup>, W. Kang<sup>2</sup> & Y.-C. Kim<sup>1</sup> ( <sup>1</sup> Yonsei Univ., <sup>2</sup> Kyunghee Univ., Korea )

$\mu$  Cassiopeiae A & B is  
- a nearby spectroscopic binary  
-  $(M_A, M_B) \sim (0.8M_{\odot}, 0.5M_{\odot})$

Mass Ratio  
Chemical composition  
Evolutionary status

is **still uncertain !!!**

In this study

Recent Observations

HIPPARCOS astrometry

CHARA optical interferometry

Spectroscopic Observation

High resolution spectroscopy (BOES)

Theoretical Modellings

Abundance Analysis

Determination of chemical composition

Evolutionary Computation

Calibration of global parameters

Asteroseismological Analysis

Internal Structure & mode- frequency

3-D R-HD Simulations

Detailed description of physical processes in atmospheres

## **SEASONAL VARIATION OF TOTAL ELECTRON CONTENT AT A TERRESTRIAL POINT WITHIN EQUATORIAL ANOMALY REGION**

Fayose, R. Sola.

Department of Physics and Electronics, Adekunle Ajasin University, Akungba Akoko, Nigeria

*Email: sola,fayose@gmail.com*

Abstract

Increasing application of Global Navigational Satellite Systems GNSS has further strengthened interest in understanding of ionospheric scintillations as a result of its impact on GNSS signals. GNSS offer a remarkable new way to study ionospheric structure and associated perturbations. The monitoring of Ionospheric Scintillation and variability of Total Electron Content TEC over a terrestrial point within equatorial anomaly region has been achieved by using the NovAtel GSV 4000B GPS-SCINDA system at Akure ( $7.3^{\circ}\text{N}$ ,  $5.2^{\circ}\text{E}$ ), Nigeria. This system is capable of tracking up to 14 GPS satellites simultaneously. Seasonal variations of Total Electron Content within the equatorial anomaly region were examined. TEC maximises in daytime at about local noon and exhibits seasonal redistribution.

# Detailed Abundance Analysis for Planet Host Stars

Wonseok Kang<sup>1</sup>, Sang-Gak Lee<sup>2</sup>, Kiehunn Bach<sup>3</sup>, Kang-Min Kim<sup>4</sup>

<sup>1</sup> *School of Space Research, Kyung Hee University, Gyeonggi-do 446-701, Republic of Korea*

<sup>2</sup> *Department of Physics and Astronomy, Seoul National University, Seoul 151-747, Republic of Korea*

<sup>3</sup> *Yonsei University Observatory, Seoul 120-749, Republic of Korea*

<sup>4</sup> *Korea Astronomy and Space Science Institute, Daejeon 305-348, Republic of Korea*

## ABSTRACT

We have obtained the spectra of 166 F, G, K type stars including 93 planet host stars using BOES (BOAO Echelle Spectrograph) with BOAO 1.8 m telescope. The spectroscopic parameters for model atmosphere were determined by self-consistent fine analysis of Fe lines. By the measurements of equivalent widths (EWs), we estimated the abundances of 25 elements including n-capture elements, such as C, N, O, Na, Mg, Al, Si, K, Ca, Sc, Ti, V, Cr, Mn, Co, Ni, Cu, Zn, Sr, Y, Zr, Ba, Ce, Nd, and Eu. And the S abundance was determined by synthetic spectrum of triplet lines near 6757 Å. For abundance analysis, the accuracy of EW measurement is very important so that we have developed the TAME (Tool for Automatic Measurement of Equivalent-width) for fast and uniform measurement of a large set of EWs.

As a results, we have confirmed that the mean metallicity of planet host stars are 0.13 dex higher than that of comparison stars. For elements other than iron, we have found that the mean value of [Mn/H] ratio for planet host stars are as much as 0.22 dex higher than for comparisons. And we note that the difference of mean [X/H] ratio is more than 0.15 dex for Na, Co, N, Al, Cu, Ni, Sc, and Si, in order of difference. Furthermore, we have performed the Kolmogorov-Smirnov test (K-S test) for [X/H] ratios between two groups of planet host stars and comparison stars and investigated the proportion of planet host stars to all samples in each bin of [X/H] ratio. As a result, we find that it is fairly not possible that the distribution of [X/H] belonged to the same population, for the elements of O, Na, Mg, Al, Si, and Zn. And we observe that the proportion of planet host stars is increasing with [X/H] ratios as an exponential function for C, O, Mg, Si, S, Ca, Sc, Cr, and Zn.

In addition to this, the opacities and equation of states (EOS) of the chemical mixtures have been calculated from the elemental analysis. Then, the evolutionary phases of the planet host stars have been computed in the context of standard stellar models. Between theoretical model grids, the detailed physical dimensions of the best model have been determined.

**Keywords :** stars: chemical abundances — stars: fundamental parameters — stars: planetary systems

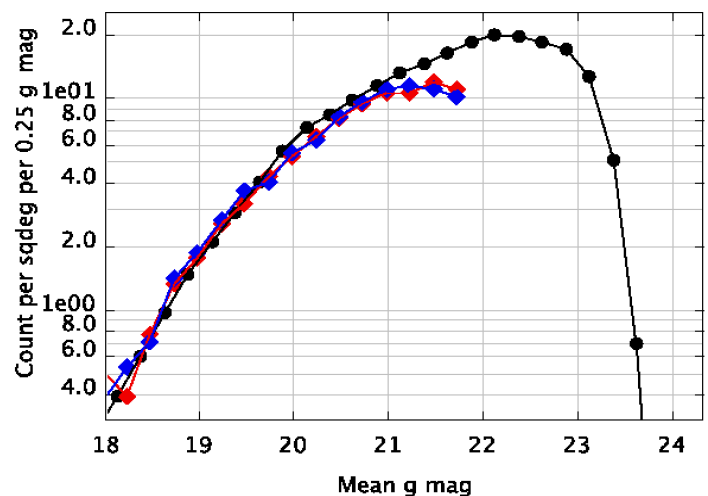
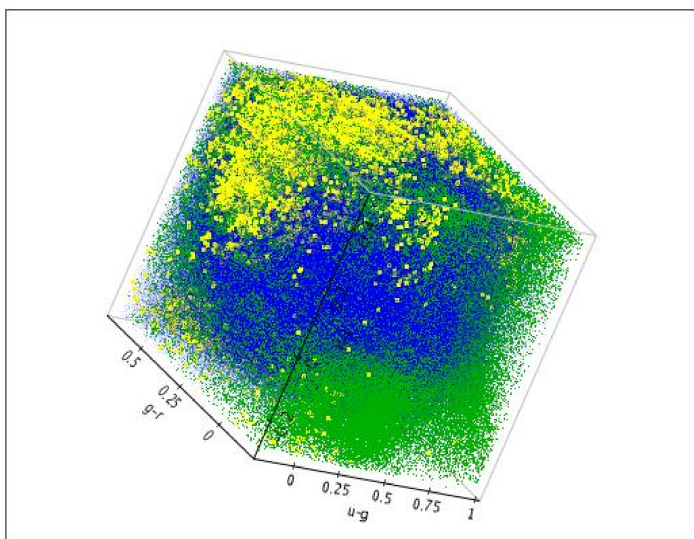
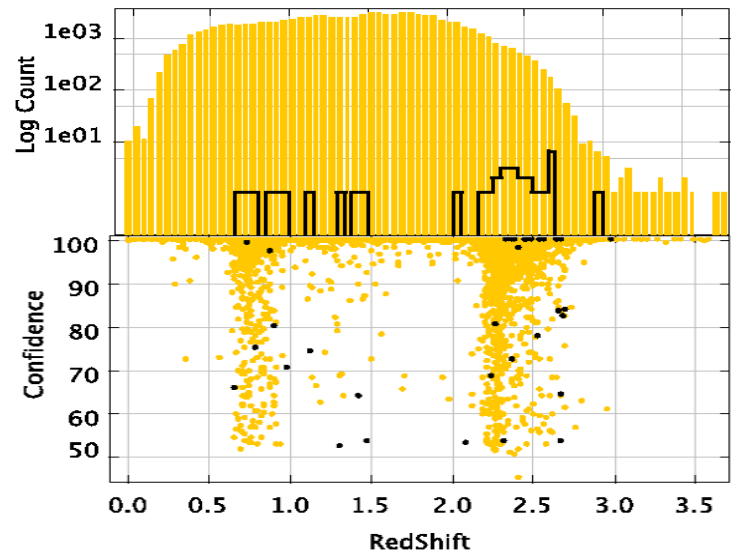
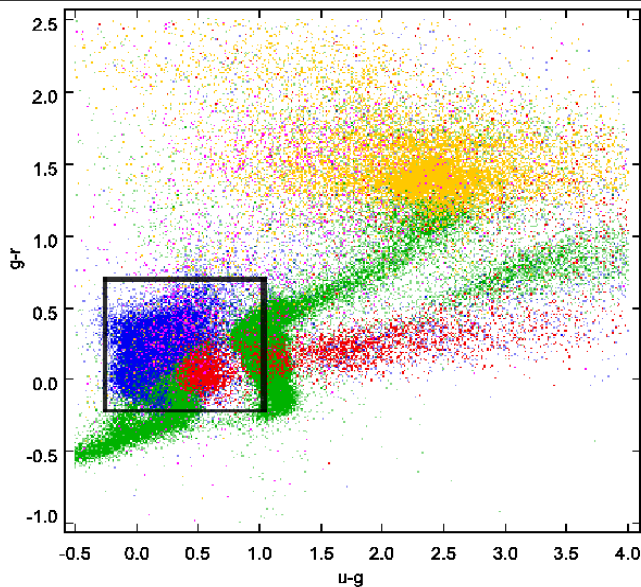
# A Difference Boosting Approach for the Photometric Detection of Point Sources From Multi - Band Survey

Sheelu Abraham<sup>1</sup>, Ninan Sajeeth Philip<sup>1</sup>, Ajit Kembhavi<sup>2</sup>

<sup>1</sup> St. Thomas College, Kozhencheri, India, <sup>2</sup> IUCAA Pune, India



We present the classification of 6 million objects from Sloan Digital Sky Survey



## Results :

- ◆ We have identified 2,430,625 quasars, 3,544,036 stars and 63,586 galaxies
- ◆ Our algorithm recovers 99.96% of spectroscopically confirmed quasars and 99.51% of stars to SDSS i-band  $\sim 21.3$  in the colour window.
- ◆ We have identified specific redshift bands where the colours of quasars, galaxies and some stars become indistinguishable.
- ◆ We show that the number density of quasars in our predictions closely agree with the theoretical estimates.
- ◆ We compared our predictions with 24 other spectroscopic surveys and find that the predictions closely agree with observations

# Figure-ground reversal about "type-behavior" and "token-behavior" in plays (Analyzed by rough sets derived lattices).

Tetsuya Matsui, Kobe-uni

## Hunter : the oldest story tellar

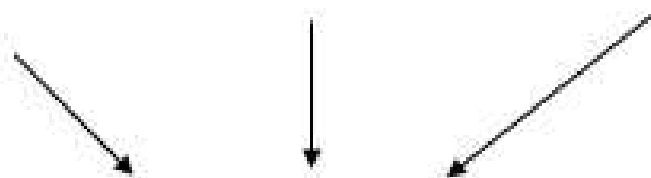
Carlo Ginzburg (1988)  
(historian)

③ The hunter guesses where the game is.

① Traces (token)



② Story to track the animal (type)





# AN UPPER LIMIT ON THE BLACK HOLE MASS FOR OPTICALLY DARK X-RAY BRIGHT SOURCES IN NEARBY GALAXIES

**Jithesh. V**  
**Department of Physics, University of Calicut, Kerala, India**

**INTRODUCTION** : Compact, off-nuclear X-ray point sources in nearby galaxies with luminosities  $10^{39}$ –  $10^{41}$  ergs/sec are called Ultra-luminous X-ray sources (ULXs).

- The observed luminosities of ULX sources exceeds the Eddington limit for a  $10M_{\odot}$  black hole. Since ULXs are off-nuclear sources, their masses must be  $< 10^5M_{\odot}$  from dynamical friction arguments.
- Thus the allowed black hole mass range for X-ray sources in nearby galaxies span five orders of magnitude ( $10M_{\odot} < M < 10^5M_{\odot}$ ) and it is important to obtain tighter constrains.

**ANALYSIS & RESULTS** : We selected the point sources from a sample of 13 elliptical galaxies from Devi *et al.* (2007) and Swartz *et al.* (2004) and optical counterparts were searched on the available archival *HST* data.

- A total of 84 point sources were analyzed in 13 elliptical galaxies and fifty six of them are having possible optical counterparts in their respective position. Twenty eight sources have no optical counterparts and named as *optically dark X-ray sources*.
- These sources are most likely to be bright X-ray binaries within the galaxy and we estimate the upper limit on their optical flux based on the  $3\sigma$  threshold at that position.
- An accretion disk around a compact object should also produce optical emission whose flux can be estimated by the standard accretion disk theory.
- For optically dark sources, the predicted accretion flux should be less than the measured upper limit. Thus one can estimate an upper limit on black hole mass (See Table).

**The Upper limit of Black hole Mass of the Optically Dark X-ray Sources**

Galaxy	<i>R.A.(J2000)</i>	<i>Decl.(J2000)</i>	$\log L_x$	$F_V \times 10^{-30}$	$M_U(M_{\odot})$
NGC4486	12 30 50.82	+12 25 02.66	$39.17^{+0.05}_{-0.04}$	0.409	1244
NGC4697	12 48 33.20	-05 47 41.17	$38.84^{+0.06}_{-0.05}$	0.752	2890
NGC4649	12 43 41.90	+11 34 33.83	$38.91^{+0.47}_{-0.11}$	0.402	3073
NGC4374	12 25 01.54	+12 52 35.59	$39.10^{+0.67}_{-0.22}$	0.441	3378
NGC1399	3 38 25.92	-35 27 42.37	$38.62^{+0.12}_{-0.09}$	0.370	3927
NGC1316	3 22 36.46	-37 13 24.68	$38.80^{+0.23}_{-0.08}$	0.449	4780
NGC1316	3 22 35.58	-37 13 14.10	$38.78^{+0.40}_{-0.07}$	0.520	6366
NGC1399	3 38 32.33	-35 26 45.73	$38.54^{+1.13}_{-0.41}$	0.377	7829
NGC1399	3 38 27.62	-35 26 48.76	$39.42^{+0.16}_{-0.14}$	0.766	7829
NGC4649	12 43 34.17	+11 33 41.93	$39.04^{+0.10}_{-0.11}$	0.912	8073

**CONCLUSIONS** : **These optically dark X-ray sources cannot be foreground stars and are highly unlikely to be background AGNs.**

- **The non-detection of optical emission impose an upper limit on the black hole mass  $M_U$ . For ten sources  $M_U < 10^4M_{\odot}$  and for one of the bright ULX sources in NGC 4486, the black hole mass is smaller than  $1244M_{\odot}$ .**
- **This is two orders of magnitude smaller than the constrain obtained from dynamical friction arguments,  $10^5M_{\odot}$ .**

# The shock chemistry of phosphorus in the L1157 B1 shocked region

T. Aota, Y. Aikawa

Department of Earth and Planetary Sciences, Kobe University,  
Kobe 657-8501, Japan

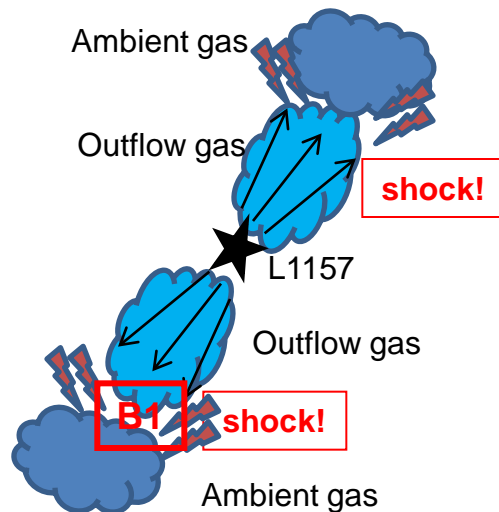
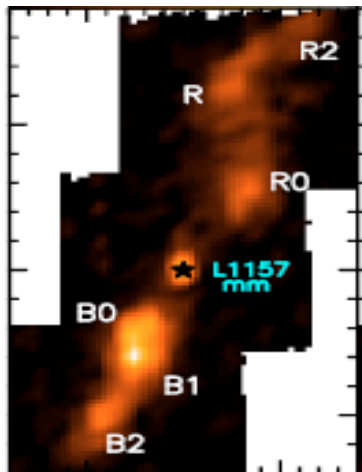
## L1157 B1 and Detection of PN

- L1157 : protostar driving a molecular outflow gas
- B1 : shocked region



Nobeyama 45m line survey

detection of PN for the first time in L1157 B1  
(Yamaguchi et al.(2011))

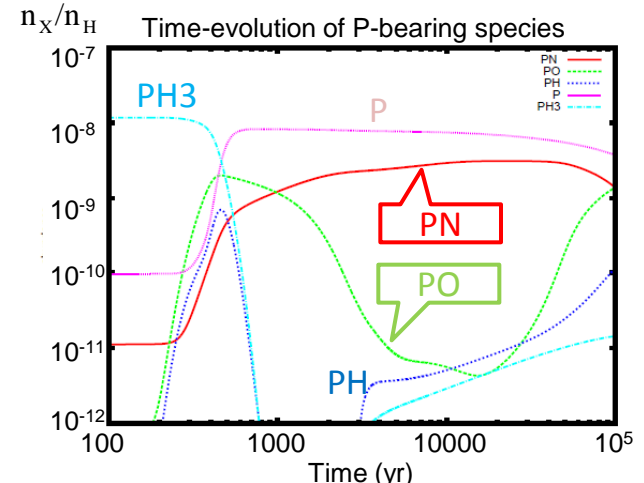
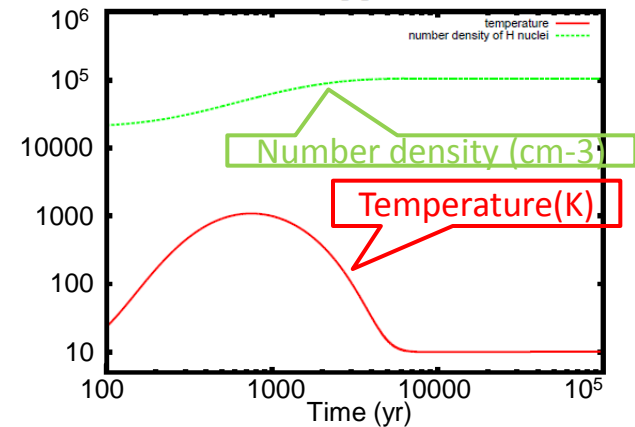


H<sub>2</sub>O 179 $\mu$ m emission along  
L1157 outflow ( Nisini et al. 2010 )

## Phosphorus chemistry in the shocked region

**Observed abundance of PN & PO are reproduced in  
C-shock models**

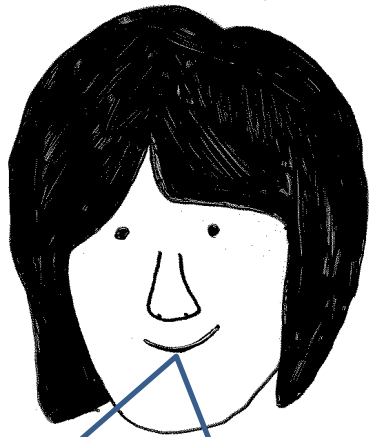
Time-evolution of temperature and number density of H nuclei



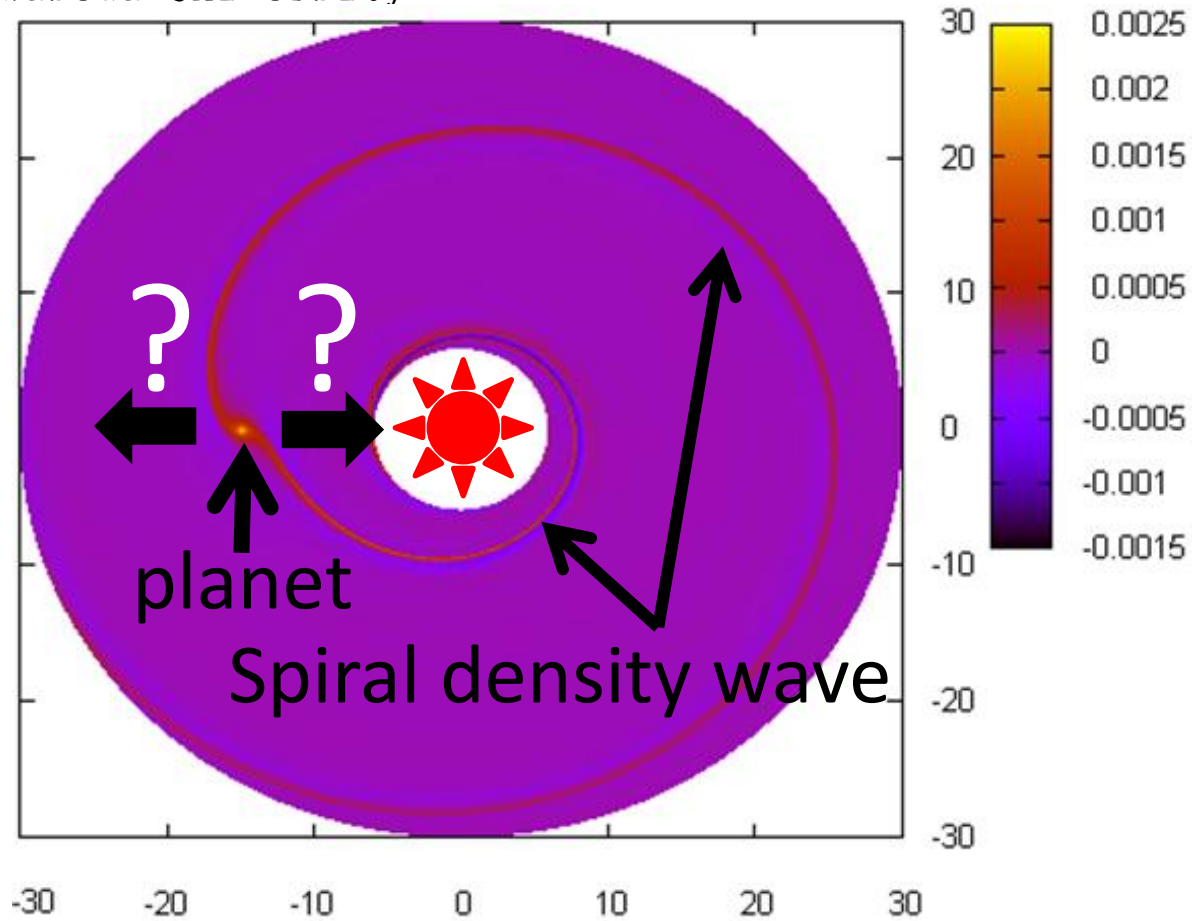
# Type I migration in an optically thin disk

K. Yamada<sup>(1)</sup> • S. Inaba<sup>(2)</sup>

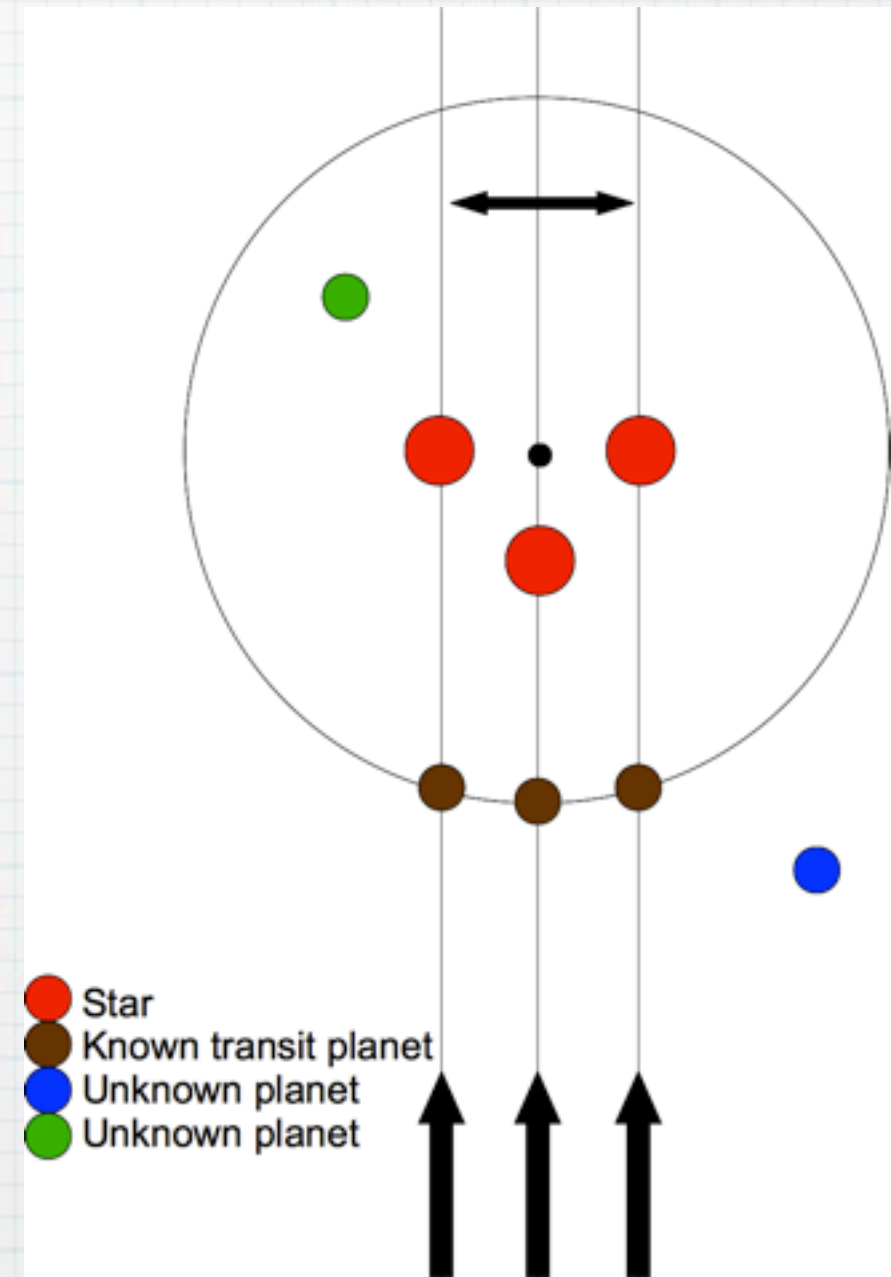
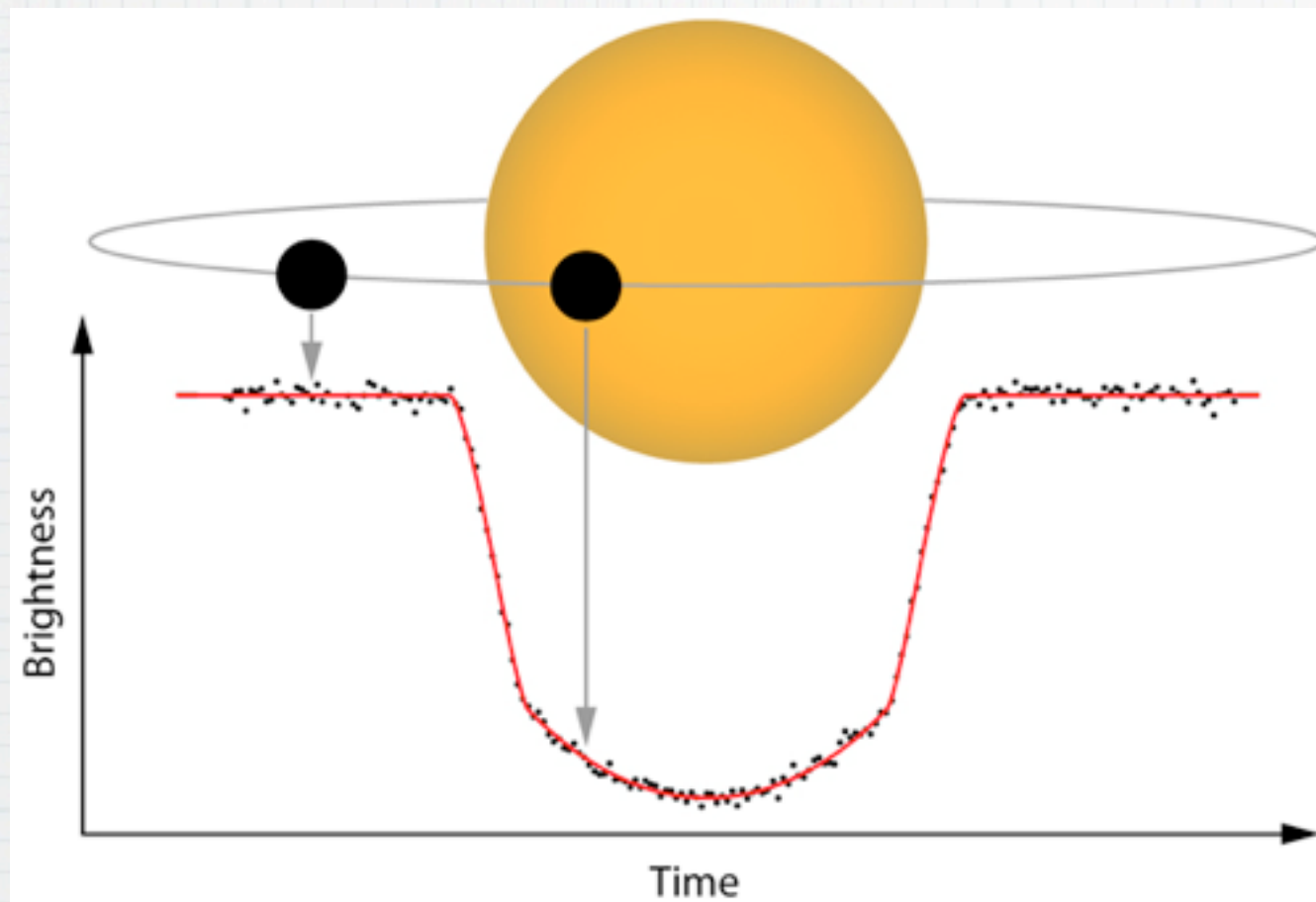
(1) CPS/Kobe University, (2) Waseda University



**OUTWARD or  
INWARD  
migration?**



# Search for unknown exoplanets by detection of transit timing variations



Sho Manabe (Kobe University)

Yoichi Itoh (Kobe University)

Noriyuki Matsunaga (The University of Tokyo)

# Duration of star formation in Young Open Clusters

*Bhavya B, Annapurni Subramaniam, Kuriakose V C*

## Aim

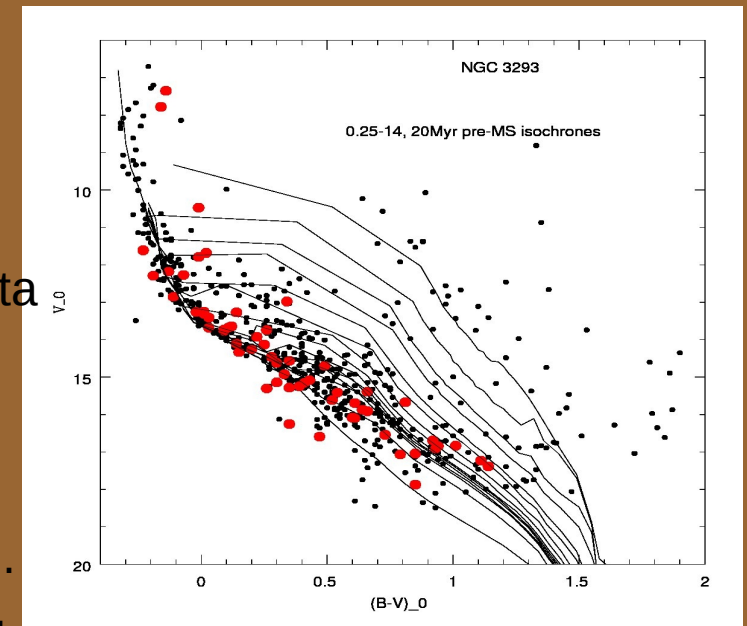
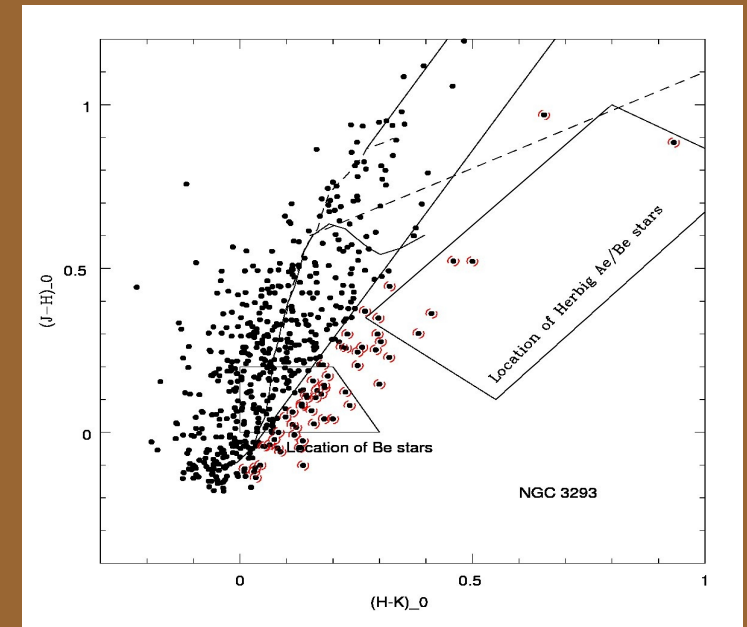
Identify young members in the cluster.  
Estimate their age and mass.  
Estimate the timescale of star formation process in the cluster.  
Estimate star formation rate within the timescale of cluster formation.

## Method

The young pre-MS stars have excess circum-Stellar emission; This property is used to identify them in Near-Infra Red (NIR) colour colour diagram.  
Ages and masses of identified PMS stars are found using stellar evolutionary models.  
The mass wise and age wise distribution is analysed to obtain the star formation snap shots.

## Results

13 young open clusters are studied using photometric data from WEBDA and NIR data from 2MASS.  
We find the presence of multiple populations inside the cluster.  
Star formation is continuous in all the clusters .  
In general, Duration timescale is equal to the cluster age .  
In some cases, low and high mass stars formed together, while in others their formation time differs.



# Near-infrared Spectroscopic Survey of the Large Magellanic Cloud with AKARI

Takashi Shimonishi  
The University of Tokyo

Infrared satellite AKARI is equipped with InfraRed Camera (IRC) which has a powerful wide-field multi-object spectroscopic capability. We have performed a spectroscopic survey of the Large Magellanic Cloud (LMC) with the IRC/AKARI.

The LMC is the nearest irregular galaxy to the Milky Way, and it is one of the few galaxies which we can obtain spatially resolved information of individual stars. So far various kinds of surveys have been performed toward the LMC. However, there are still few spectroscopic surveys in the infrared wavelength range. Infrared spectral information is necessary for the classification and the investigation of the individual spectral features of infrared bright objects, e.g. young stellar objects or mass-losing evolved stars.

As a result of the spectroscopic survey of the LMC with IRC/AKARI, we obtained 2 -- 5 micron spectra of ~3000 point sources in the LMC. In terms of the number of sources, this is the largest infrared spectroscopic survey ever performed toward the LMC. In this presentation, we introduce this survey and examples of a science with the survey data in more detail.

# Time-Frequency Analysis of Superorbital Modulation of X-ray Binary SMC X-1 by Hilbert-Huang Transform



Chin-Ping Hu<sup>1</sup>, Yi Chou<sup>1</sup>, Ming-Chya Wu<sup>2</sup>, Ting-Chang Yang<sup>1</sup>, Yi-Hao Su<sup>1</sup>



<sup>1</sup> Institute of Astronomy, National Central University, Taiwan

<sup>2</sup> Research Center for Adaptive Data Analysis, National Central University, Taiwan

## Abstract

The high-mass X-ray binary (HMXB) SMC X-1 exhibits a superorbital modulation with a dramatically varying period ranging between  $\sim 40$  d and  $\sim 60$  d. This research studies the time-frequency properties of the superorbital modulation of SMC X-1 based on the observations made by the All-Sky Monitor (ASM) onboard the Rossi X-ray Timing Explorer (RXTE). We analyzed the entire ASM database collected since 1996. The Hilbert-Huang Transform (HHT), developed for non-stationary and nonlinear time series analysis, was adopted to derive the instantaneous superorbital frequency. The resultant Hilbert spectrum is consistent with the dynamic power spectrum while it shows more detailed information in both the time and frequency domains. The RXTE observations manifest that the superorbital modulation period was mostly between  $\sim 50$  d and  $\sim 65$  d, when it changed to  $\sim 45$  d around MJD 50,800 and MJD 54,000. Our analysis further indicates that the instantaneous frequency changed in a time scale of hundreds of days between  $\sim$ MJD 51,500 and  $\sim$ MJD 53,500. Based on the instantaneous phase defined by HHT, we folded the ASM light curve to derive a superorbital profile, from which an asymmetric feature and a low state with barely any X-ray emissions (lasting for  $\sim 0.3$  cycles) were observed. We also calculated the correlation between the mean period and the amplitude of the superorbital modulation. The result is similar to the recently discovered relationship between the superorbital cycle length and the mean X-ray flux for Her X-1.

## 1. Introduction

The high-mass X-ray binary (HMXB) SMC X-1, which was first discovered in 1971 (Leong et al. 1971), consists of a  $1.06 M_{\odot}$  neutron star (van der Meer et al. 2007) and a B0 I type supergiant with a mass of  $17.2 M_{\odot}$ . The spin period of the neutron star is 0.71 s (Wojdowski et al. 1998) and the orbital period of this system is  $\sim 3.89$  d as evaluated by its eclipse (Schreier et al. 1972).

SMC X-1 exhibits a superorbital modulation with its period changes between  $\sim 40$  d and  $\sim 65$  d. After the All-Sky Monitoring (ASM) onboard the Rossi X-ray Timing Explorer (RXTE) collected sufficient amounts of data, several time-frequency analysis methods such as the wavelet transform (Ribó et al. 2001), dynamic power spectrum (Clarkson et al. 2003), and sliding Lomb-Scargle periodogram (Trowbridge et al. 2007) were applied to the light curve to investigate the variations in the superorbital period of SMC X-1. The mechanism of superorbital modulations in SMC X-1 are interpreted by a warped and tilted accretion disk (Wojdowski et al. 1998). When the disk precesses, it obscures our line of view to the central X-ray source.

## 2. Data Analysis

### 2.1 RXTE ASM

Since the RXTE was launched in late 1995, the ASM continuously sweeps the entire sky once every 90 minutes. The energy range of the ASM is 1.3 to 12.1 keV. This can be further divided into three energy channels (ch1: 1.3-3.0 keV, ch2: 3.0-5.0 keV, and ch3: 5.0-12.1 keV). The summed band data collected from 1996 to 2010 (MJD 50134 to MJD 55371), with a total time span of  $\sim 5000$  d were used in this time-frequency analysis. The dwell data, where all the eclipses were removed according to the ephemeris proposed by Wojdowski et al. 1998, were binned into a one-day averaged light curve.

### 2.2 Hilbert-Huang Transform

Owing to the high variability of the superorbital cycle length of SMC X-1, it is suitable to analyze the time-frequency properties of its superorbital modulation by the HHT. HHT, established in 1998 (Huang et al. 1998), is an adaptive data analysis method that can detect the frequency changing with time instantaneously. The procedure of HHT is divided into two steps: decomposing the original data into intrinsic mode functions (IMFs) and applying Hilbert transform or other method on the IMFs to obtain the instantaneous frequencies and amplitudes. Thus, the original light curve  $x(t)$  can be represented as:

$$x(t) = \sum_{j=1}^n a_j(t) \exp\left(i \int_0^t \omega_j(t') dt'\right)$$

where  $a_j(t)$  and  $\omega_j(t)$  are the instantaneous amplitudes and frequencies of decomposed components.

The RXTE/ASM lightcurve was decomposed into IMFs by Ensemble Empirical Mode Decomposition (EEMD) method (Wu et al. 2009). The decomposition result is shown as Figure 1. The significance test (Wu et al. 2004) on these IMFs suggests that the 40 -- 60 d superorbital modulation signal of SMC X-1 mostly concentrates in the fifth component ( $c_5$ ). The values of all the other components are lower than or marginal at the  $3\sigma$  white noise level, suggesting that they act in a manner similar to white noise. These components are probably caused by the observational noise associated with non-periodic modulations in other time scales.

## 3. Result

### 3.1 Hilbert Spectrum

After decomposing the ASM light curve into IMFs, the normalized Hilbert transform (Huang & Long 2003) was applied on the IMFs to obtain the instantaneous frequencies and amplitudes. The resultant Hilbert spectrum is a three-dimensional map which displays how the modulation period and amplitude vary with time. Figure 2 shows the result, in which the frequency range is divided into 3000 bins and the spectrum is smoothed by a Gaussian filter for clarity. The color map represents the Hilbert energy spectrum with the magnitude of energy defined as square of the amplitude. For comparison, the dynamic power spectral technique, as described in Clarkson et al. (2003), was also applied on the ASM light curve. It is obvious that the Hilbert energy spectrum is consistent with the dynamic power spectrum. Because the spectral analysis based on HHT is independent of window size, more detailed structures in the light curve data can be observed from the high-resolution Hilbert spectrum than the dynamic power spectrum.

## References

Clarkson, W. I., et al. 2003, MNRAS, 339, 447  
 Hickox, R. C., & Vrtilak, S. D. 2005, ApJ, 633, 1064  
 Huang, N. E. et al. 1998, Proc. R. Soc. Lond. A, 454, 903  
 Huang, N. E., & Long, S. R. 2003, NASA Patent Pending GSC 14,673-1  
 Leong, C., et al. 1971, ApJ, 170, L67

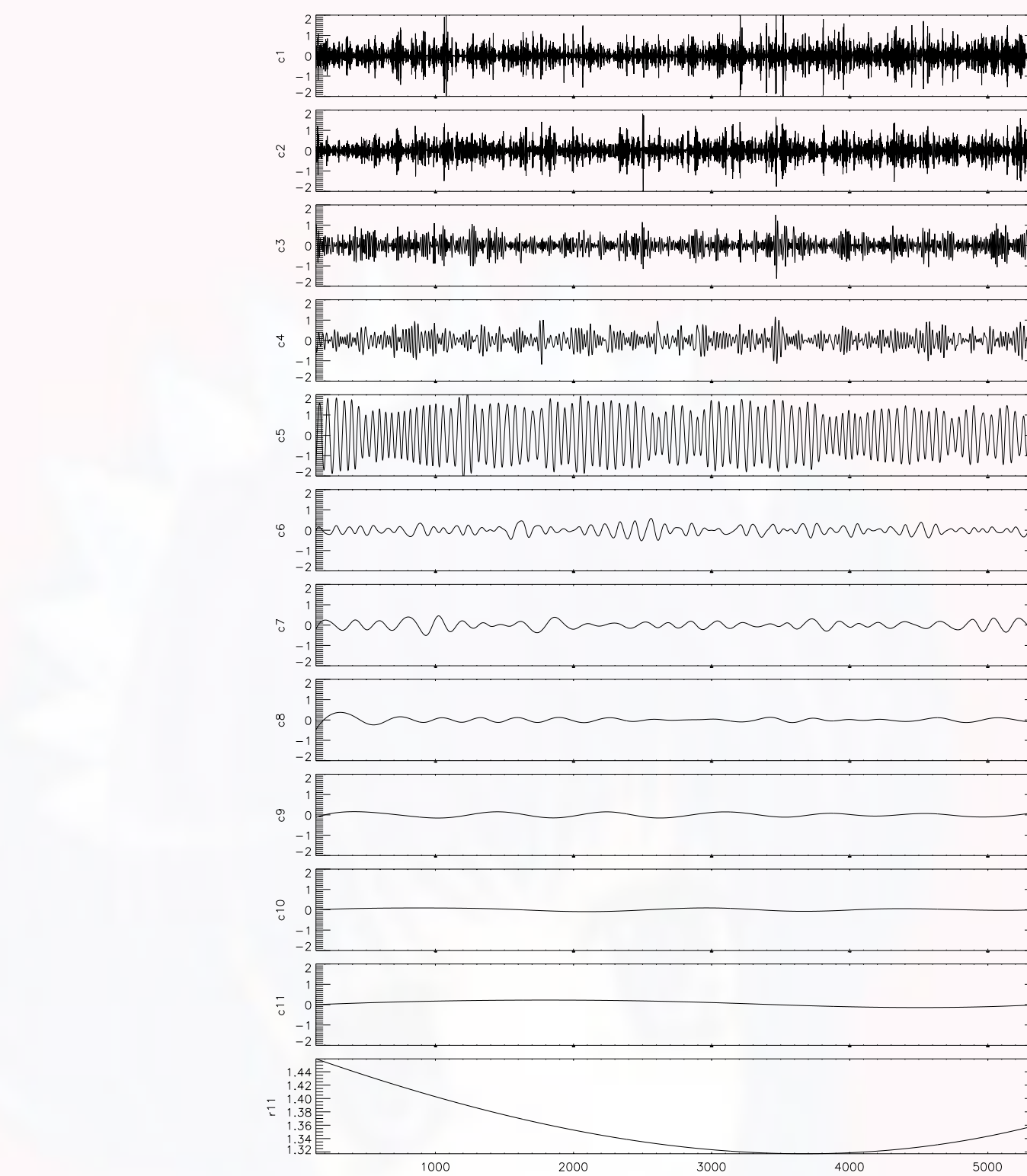


Figure 1. Intrinsic mode functions (IMFs) decomposed by ensemble empirical mode decomposition (EEMD). The fifth IMF ( $c_5$ ) is responsible for the  $\sim 40$  d to  $\sim 60$  d superorbital modulation.

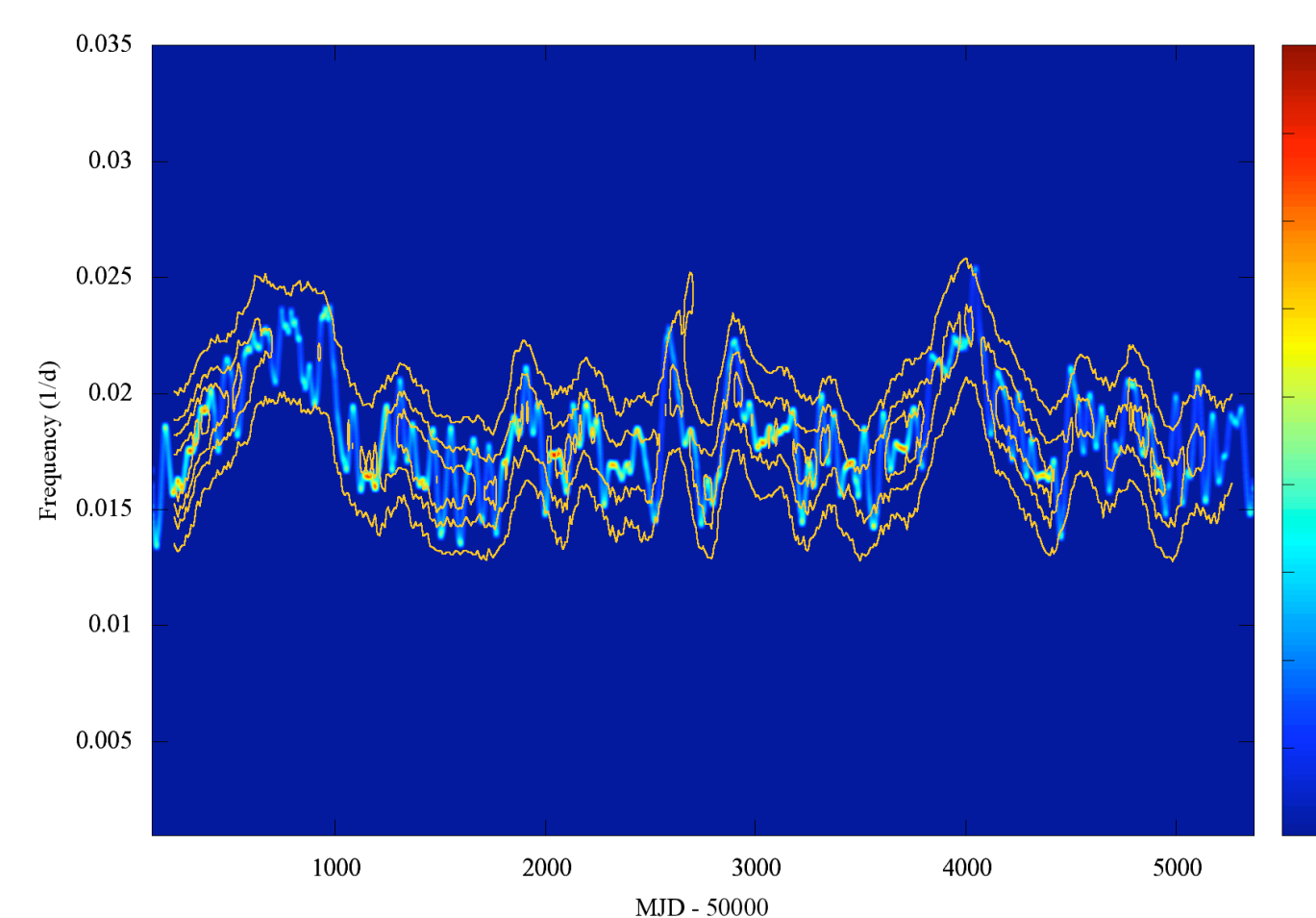


Figure 2. Hilbert energy spectrum (color map) and dynamic power spectrum (contour plot). The blue curve represents the instantaneous frequency of IMF  $c_5$  after Gaussian smoothing and the color depth denotes the magnitude of the Hilbert energy.

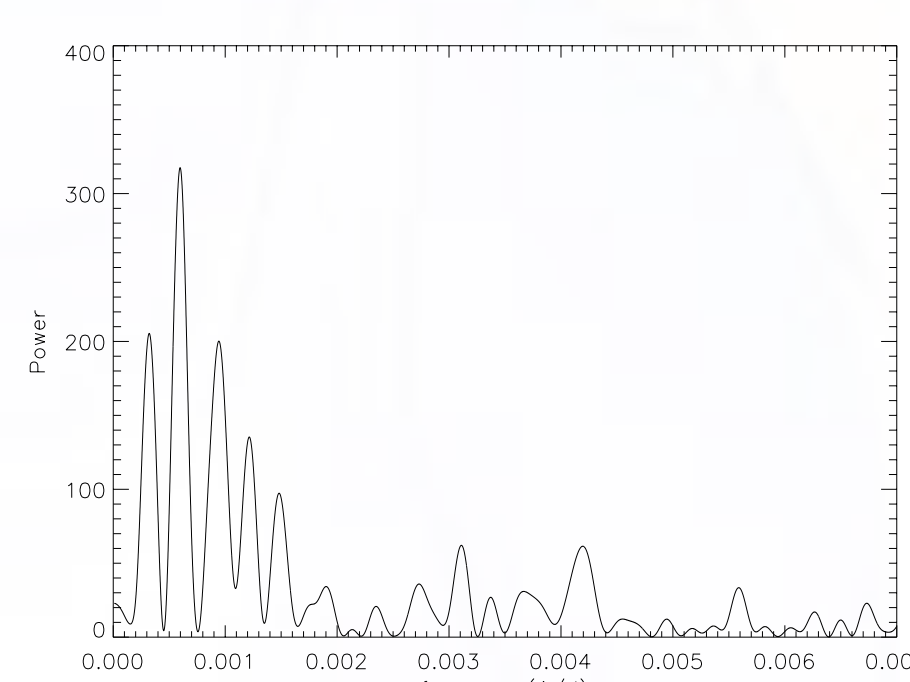


Figure 3. Lomb-Scargle periodogram of the instantaneous frequency of IMF  $c_5$ . The highest peak is located at  $f \sim 0.0006$  (or  $P=1647$  d), which is the second harmonic of  $P \sim 3200$  d peak. The other prominent peaks are located at  $P \sim 240$  d and  $P \sim 320$  d.

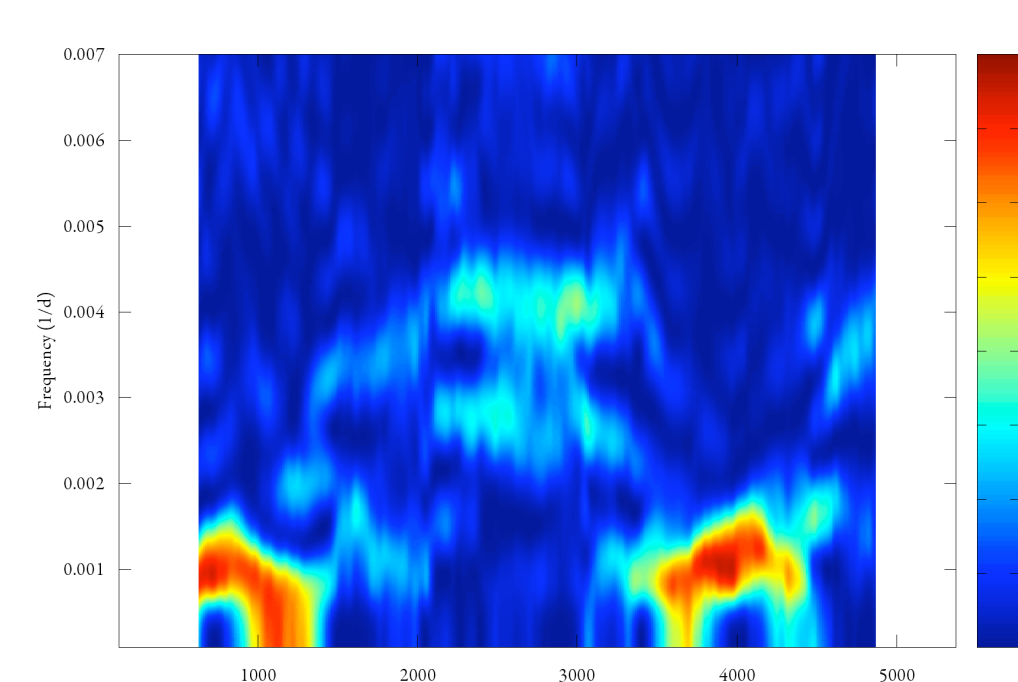


Figure 4. Dynamic power spectrum of the instantaneous frequency of IMF  $c_5$ .

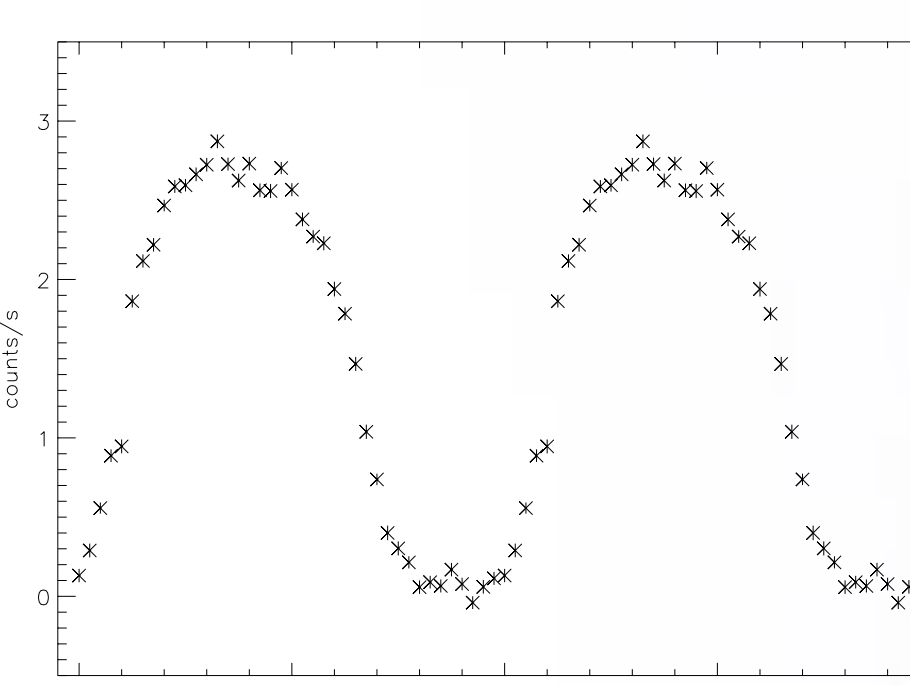


Figure 5. Folded light curve of SMC X-1 according to the phase defined by HHT. The number of bins in one cycle is 40.

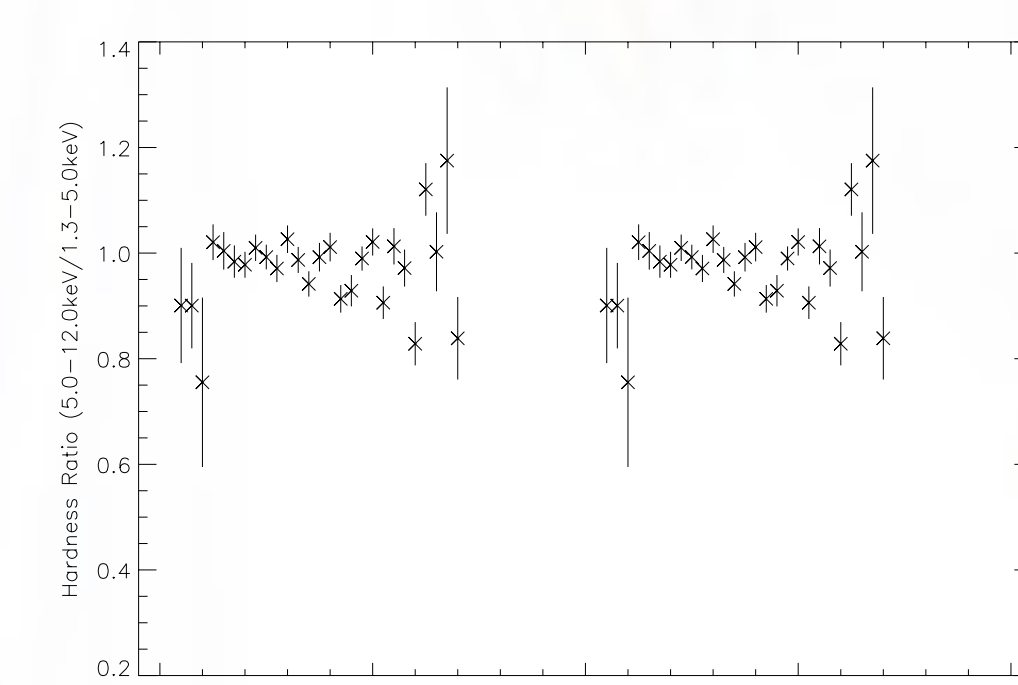


Figure 6. Hardness ratios folded according to the superorbital phase. Only the data points with a signal to noise ratio greater than 5 were chosen to calculate the hardness ratios.

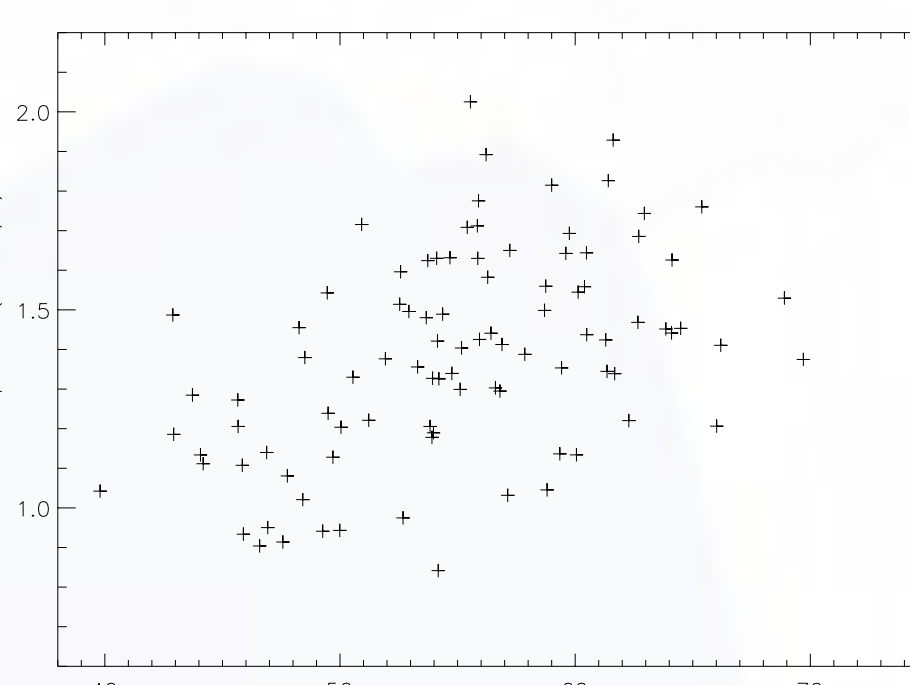


Figure 7. Correlation of cycle-averaged period and Hilbert amplitude of IMF  $c_5$ .

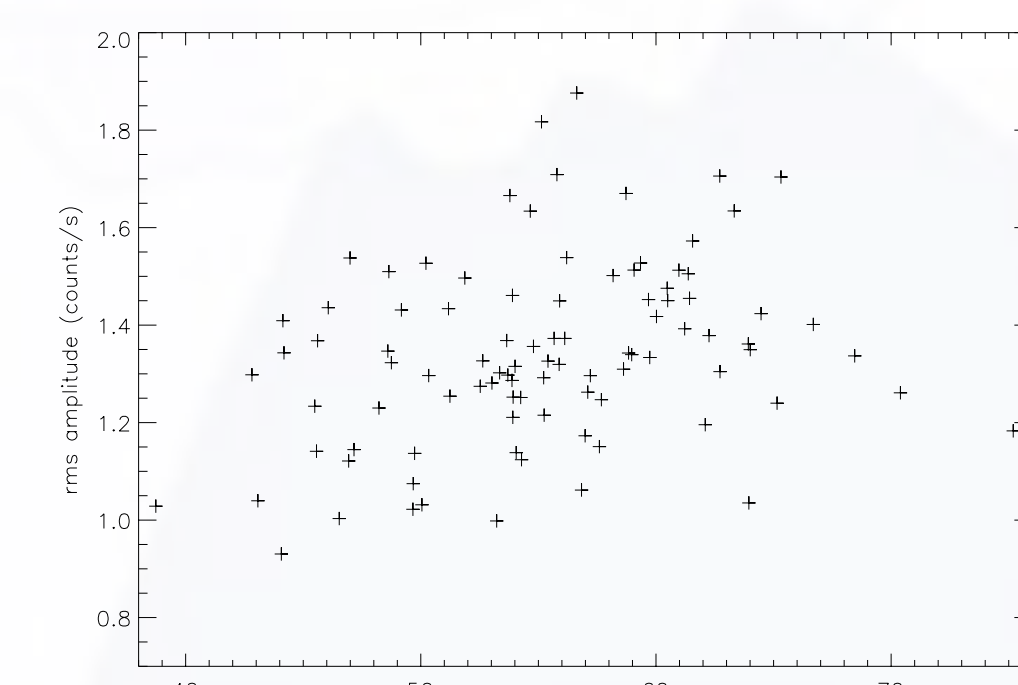


Figure 8. Correlation of cycle-averaged period and rms amplitude of original ASM light curve.

The first remarkable feature of both spectra is that the superorbital modulation period changes dramatically from  $\sim 60$  d to  $\sim 45$  d and goes back to  $\sim 60$  d between  $\sim$ MJD 50,200 and  $\sim$ MJD 51,100. Interestingly, a similar variation in the superorbital modulation period is repeated between  $\sim$ MJD 53,600 and  $\sim$ MJD 54,400. The time durations of these two events are roughly 800 d and the separation between them is  $\sim 3200$  d. This indicates that such a phenomenon is probably recurrent. In addition, although the superorbital period is relatively stable, it seems to oscillate between  $P \sim 50$  d and  $\sim 65$  d over a time scale of hundreds of days between  $\sim$ MJD 52,000 and  $\sim$ MJD 53,000. The Hilbert spectrum displays the instantaneous frequency more accurately, enabling the application of further timing analysis methods on the instantaneous frequency to assess the periodicity hidden in the superorbital period change.

In order to study the periodicities in the variation of the superorbital frequency, the Lomb-Scargle periodogram was applied on the instantaneous frequency of the component  $c_5$ , and the result is shown in Figure 3. The highest peak is located at  $P = 1674$  d; this is consistent with the previously reported periodicity (Ribó et al. 2001, Clarkson et al. 2003). However, this peak is the second harmonic of  $P \sim 3200$  d, and it corresponds to the separation of the events occurring when the superorbital period changes between  $\sim 60$  d and  $\sim 45$  d. Moreover, a few peaks with relatively less power values located at  $P \sim 240$  d and  $P \sim 320$  d are observed. Figure 4 shows a dynamic power spectrum with a window size of 1,000 d and a movement of 10 d. The most prominent peaks are located at around MJD 50,800 and MJD 54,000. These peaks correspond to the short-period state of the superorbital modulation in the time domain in Figure 2 and the highest peaks in the frequency domain in Figure 3.

### 3.2 Superorbital Profile

It is difficult to derive a proper profile to describe the characteristics of superorbital modulation for highly variable cycle lengths from a light curve folded with a fixed period. From Hilbert transform, a well-defined phase of  $\phi(t) = \theta(t)/2\pi$  can be easily obtained even if the period changes dramatically. Figure 5 shows the folded light curve of SMC X-1, and the phase zero epoch is defined by the first data point in the light curve (MJD 50,134).

The major distinction between this superorbital modulation profile and that obtained from previous studies is a clear low state with a negligible X-ray flux lasting for  $\sim 0.3$  cycle. Moreover, the asymmetric features of the superorbital profile can also be obtained in the folded light curve. By calculating the time scale between 10% and 90% of amplitude, the rising time scale is  $\sim 0.14$  cycle (from phase 0.05 to 0.19), which is shorter than the falling time scale of  $\sim 0.19$  cycle (from phase 0.54 to 0.73).

The ASM hardness ratio was defined as  $ch3/(ch1+ch2)$ , since  $ch3$  and  $ch1+ch2$  have similar photon count rates during the high state. Only the data with a signal to noise ratio (SNR) greater than 5 were chosen and folded according to the superorbital phase defined in HHT. The folded hardness ratio is shown in Figure 6. It is easily observed that the hardness ratios in the high state (from phase 0.19 to 0.54) are relatively stable. In the transition state (phase 0.05--0.19, and 0.54--0.73), the hardness ratios do not appear to significantly deviate from the mean value as compared with that in the high state although the errors are much greater.

### 3.3 Correlation Between Period and Amplitude

Another remarkable feature observed in this study is the correlation of the amplitude with the period. Using the instantaneous frequency and amplitude derived by HHT, the correlation between the cycle-averaged period and the Hilbert amplitude in the most significant IMF ( $c_5$ ) was calculated. The rank correlation coefficient is  $r=0.46$  with a null hypothesis probability value of  $3.2 \times 10^{-6}$ , indicating a significant correlation between the period and the amplitude (see Figure 7). In order to obtain the correlation between the period and amplitude in the original data set, the rms amplitude of each cycle was calculated. The result shows that the period and the rms amplitude still show a significant correlation ( $r=0.32$  with null hypothesis probability value of  $1.4 \times 10^{-3}$ , see Figure 8).

## 4. Summary

We have successfully performed HHT-based time-frequency analysis on the ASM light curve of SMC X-1. The Hilbert spectrum manifests variations in the instantaneous period of the superorbital modulation. The instantaneous phase defined by HHT allows us to fold the light curve to derive a reasonable superorbital profile. The time-frequency information obtained from the HHT analysis is more abundant than the traditional Fourier-based methods. This benefits our investigations on the superorbital modulation of SMC X-1.

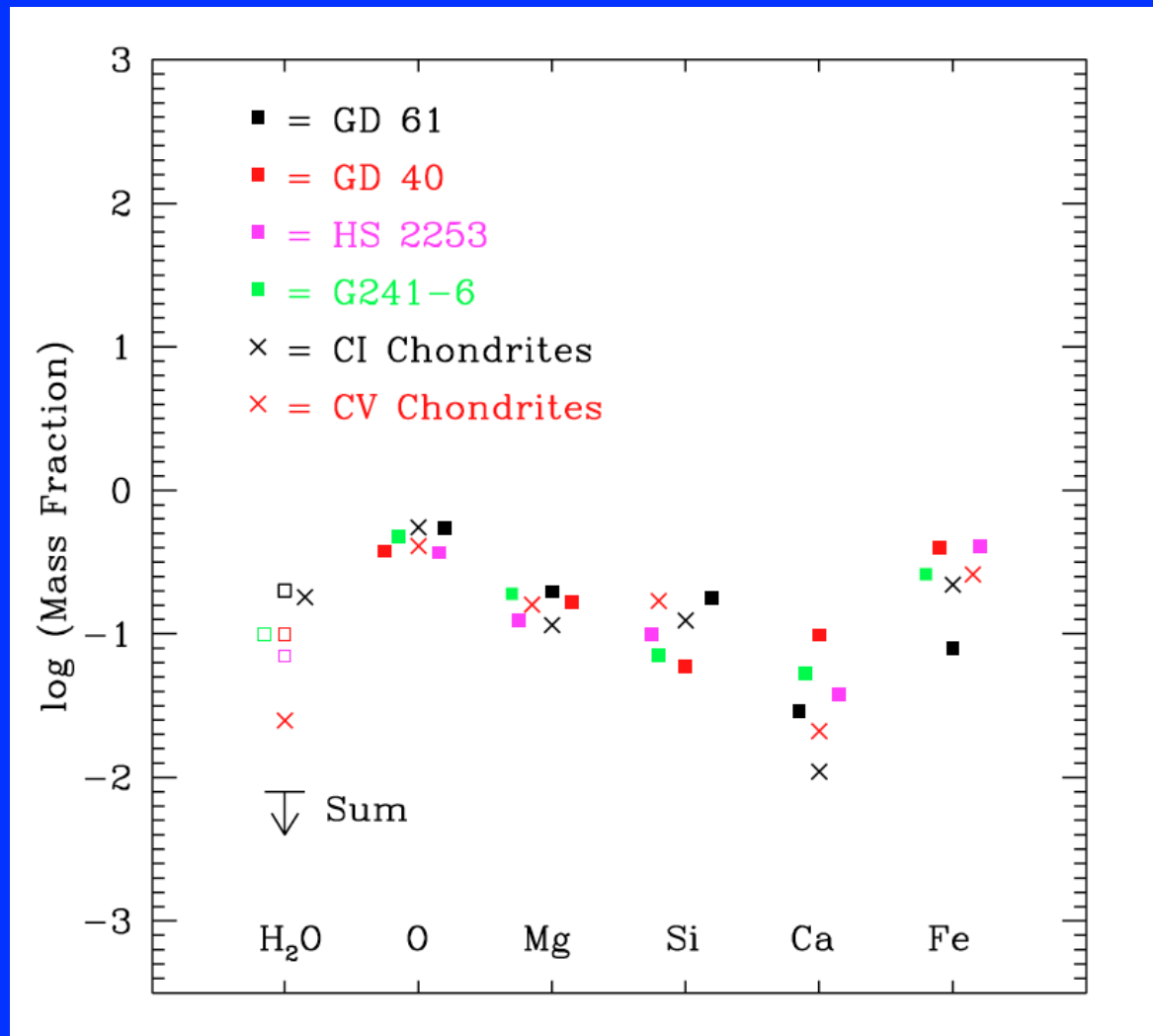
Neilsen, J., et al. 2004, ApJ, 616, L135  
 Reynolds, A. P., et al. 1993, MNRAS, 261, 337  
 Ribó, M., et al. in Proc. of Fourth INTEGRAL Workshop  
 Schreier, E., et al. 1972, ApJ, 178, L71  
 Trowbridge, S., et al. 2007, ApJ, 670, 624

van der Meer, A., et al. 2007, A&A, 473, 523  
 Wojdowski, P., et al. 1998, ApJ, 502, 253  
 Wu, Z., & Huang, N. E. 2004, Proc. R. Soc. Lond. A, 460, 1597  
 Wu, Z., & Huang, N. E. 2009, Advance in Adaptive Data Analysis, vol 1, 1

# Water in Extrasolar Rocky Planets

--derived from polluted white dwarfs

Siyi Xu (许偲艺), UCLA



# MEDIUM RESOLUTION SPECTRAL LIBRARY OF LATE-TYPE STELLAR TEMPLATES IN NEAR-INFRARED BAND

Huynh Anh Nguyen Le<sup>1</sup>, Soojong Pak<sup>1</sup>, Wonseok Kang<sup>1</sup>, Myungshin Im<sup>2</sup>, Jeong-Eun Lee<sup>1</sup>, Luis C. Ho<sup>3</sup>,  
 Tae-Soo Pyo<sup>4</sup>, Daniel T. Jaffe<sup>5</sup>

*<sup>1</sup>School of Space Research, Kyung Hee University, <sup>2</sup>Department of Physics and Astronomy, Seoul National University, <sup>3</sup>The Observatories of the Carnegie Institution for Science, <sup>4</sup>Subaru Telescope, National Astronomical Observatory of Japan, <sup>5</sup>Department of Astronomy, University of Texas at Austin*

## 1. Introduction

- The medium resolution ( $R = 5000-6000$ ) spectra in the near-infrared band  $1.4-1.8 \mu\text{m}$ , for late-type stars.
- We measured the equivalent of widths and compared our results to those of Meyer et al. (1998) (M98).
- We use the  $\text{Mg}(1.71113 \mu\text{m})$  line to estimate approximate temperature for late-type stars.

## 2. Observation, data reduction, and Results

- SUBARU 8.2 m telescope.
- Infrared Camera Spectrograph (IRCS).
- G-K-M types stars.
- Data reduction by using IRAF (Image Reduction Analysis Facilities).

## 3. Discussion

- Comparison the spectral resolution of Arcturus (K2 III).
- Discussion the results from comparing our EW results with M98.

## 4. Conclusion and Future works

- The medium resolution ( $R = 5000-6000$ ) spectra in the near-infrared band  $1.4-1.8 \mu\text{m}$ , for late-types G-K-M stars. Our spectral resolution is good enough for analysis the lines in the spectra.
- The approximate temperature of late-type stars is estimate by using absorption line  $\text{Mg} (1.71113 \mu\text{m})$ .
- The CO band head  $1.62073 \mu\text{m}$  obtained from the spectra is potentially useful for measuring the velocity dispersion in the central region of the QSO host galaxies.

